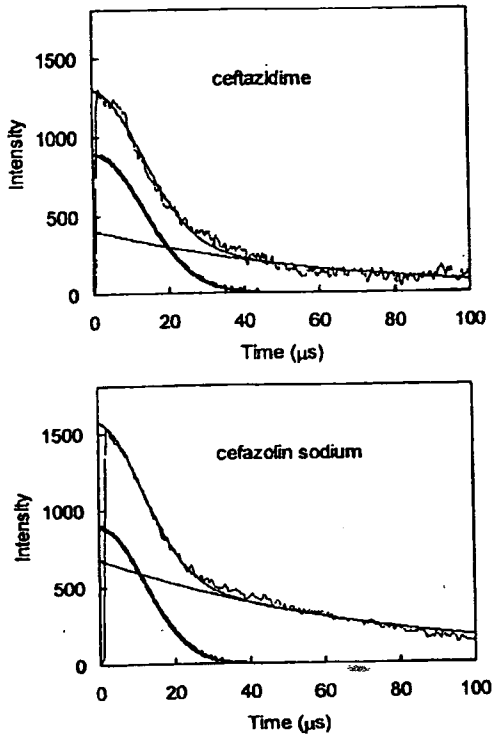

Figure 1. Free induction decay for ceftazidime and cefazolin sodium hydrates.

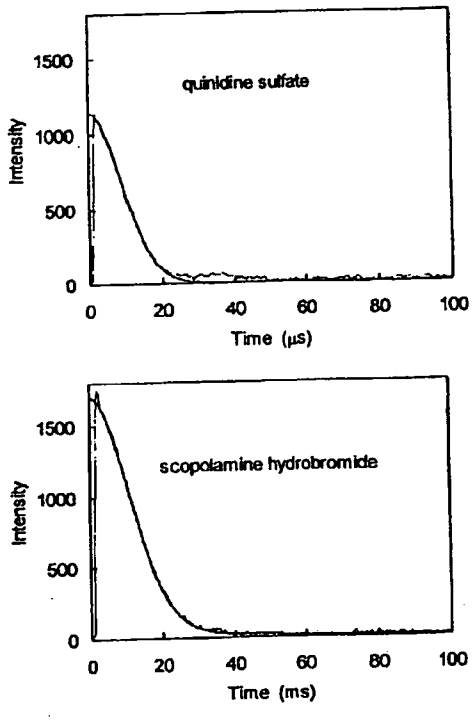

Figure 2. Free induction decay for quinidine sulfate and scopolamine hydrobromide hydrates.

spectroscopy.[8] NMR is also utilized to determine the molecular mobility of water in the solid state,[9] and to examine the various mechanisms by which solids interact with water.[10,11] However, there have been few studies in which the molecular mobility of water in API hydrates was determined using NMR. This may be because ^{1}H-NMR, even high resolution ^{1}H-NMR, cannot separate the peaks of the water protons from those of the protons in other components, which prevents specific determination of water mobility. Although the preparation of API hydrate samples using ^{17}O-labeled water allows to specifically determine the mobility of the water molecules by ^{17}O-NMR, unaffected by the other components, this approach requires high cost and much labor. Thus, determination of the molecular mobility of

Table 1. Water Content of API Hydrates

API Hydrate	Number of H_2O per Molecule Specified in JP	Number of H_2O per Molecule Determined by KF	Spin–Spin Relaxation of H_2O
Cefazolin sodium	5	4.67	Lorentzian
Ceftazidime	5	5.04	Lorentzian
Amoxicillin	3	2.94	Lorentzian
Ampicillin	3	2.96	Lorentzian
Berberine Chloride	Not specified	2.67	Gaussian
Quinine hydrochloride	2	1.31	Gaussian
Scopolamine hydrobromide	3	2.32	Gaussian
Saccharin sodium	2	1.15	Gaussian
Pipemidic acid	3	2.9	Gaussian
Sulpyrine	1	0.98	Gaussian
Quinidine sulfate	2	1.95	Gaussian

DOI 10.1002/jps

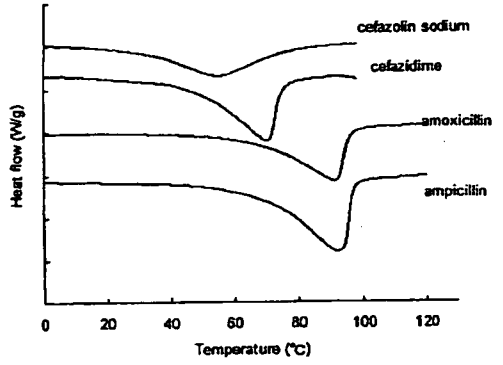

Figure 3. DSC thermograms for four antibiotic hydrates.

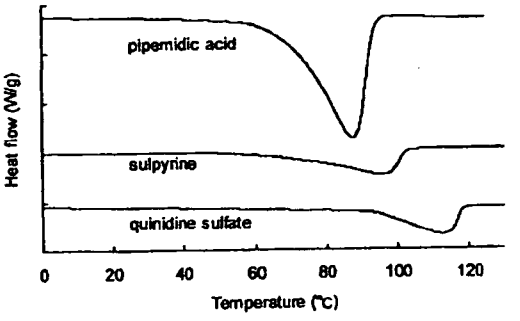

Figure 5. DSC thermograms for API hydrates showing a single endothermic peak.

hydration water in API hydrates using NMR holds some challenges.

However, it is possible to determine the molecular mobility of hydration water in API hydrates by spin–spin relaxation measurement, if the spin–spin relaxation time (T_2) of the water protons is significantly different from that of the API protons. Furthermore, the spin–lattice relaxation time (T_1) of the water protons may be a useful indicator of water mobility, if the ratio of water protons to API protons is sufficiently large, or if the water protons have a correlation time (τ_c) corresponding to the T_1 minimum, such that the T_1 of the water proton is sensitively reflected in the measured T_1 value without being affected by spin diffusion between the water and the API protons. Moreover, even if the ratio of water protons to API protons is not particularly large, and even if water proton does not have a τ_c corresponding to the T_1 minimum, it may be possible to compare the molecular mobility of hydration water in API hydrates based on measured T_1 values, if both of the T_1 of the API proton and the ratio of water protons to API protons are similar for all of the API hydrates compared.

The purpose of this study was to examine the possibility of determining the molecular mobility of hydration water in API hydrates by NMR relaxation measurement. Spin–lattice relaxation, which reflects motions of MHz order, and spin–spin relaxation, which reflects slower motions, were measured for the 11 API hydrates listed in the Japanese Pharmacopeia (JP) using pulsed ^{1}H-NMR, which allows more simplified measurements than high-resolution ^{1}H-NMR. Furthermore, the ease of evaporation of the hydration water was determined under nonisothermal and isothermal conditions using DSC and water vapor sorption isotherm analysis, respectively, and the relationship between the ease of evaporation and the measured values of T_1 and T_2 was examined.

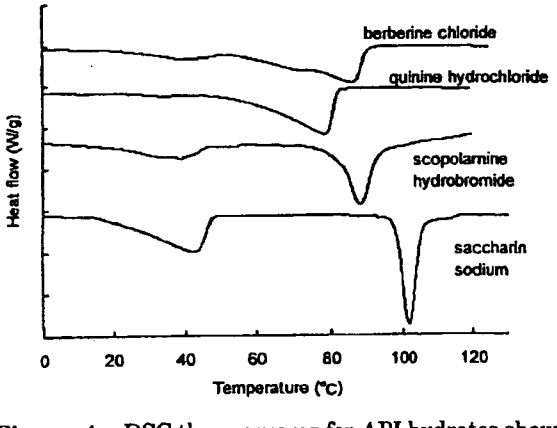

Figure 4. DSC thermograms for API hydrates showing two endothermic peaks.

EXPERIMENTAL

Materials

Cefazolin sodium, ceftazidime, amoxicillin, ampicillin, scopolamine hydrobromide, pipemidic acid, quinidine sulfate hydrates were purchased from Sigma[Q2], and berverine chloride, quinine hydrochloride, saccharin sodium, sulpyrine and di-sodium hydrogen phosphate 12 H_2O were purchased from Wako[Q3], and di-sodium hydrogen phosphate 2 H_2O was from Merck[Q4].

DOI 10.1002/jps

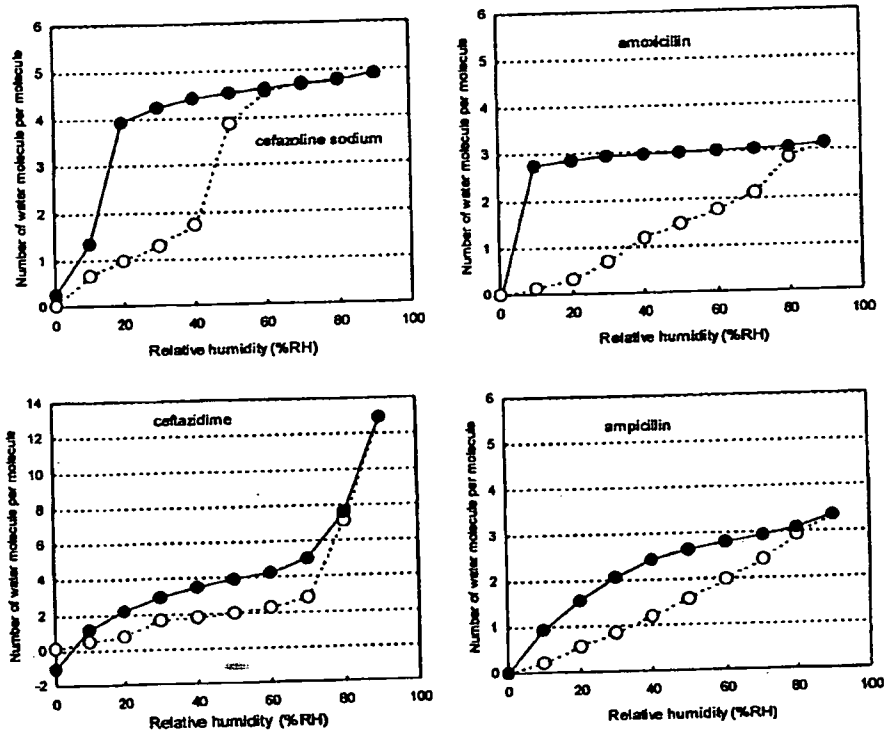

Figure 6. Water sorption isotherms for four antibiotic hydrates.

NMR Relaxation Times

The free induction decay (FID) of protons in API hydrates was obtained using a pulsed NMR spectrometer (25 MHz, JNM-MU25, JEOL, Tokyo, Japan). FID was obtained at 10, 20, 30, and 40°C. The 90° pulses were 2 μs in duration. The "solid echo," with an echo delay of 10 μs, was used in the detection stage of all measurements, in order to overcome the effects of the dead-time.[12] Measurement was repeated four times with a recycling time over five times of the T_1 value measured as described below.

The FID signals obtained between 2.6 and 100 μs that showed only Gaussian-type decay were fitted to Eq. (1) to calculate the T_2 of proton. FID signals obtained for quinidine sulfate and pipemidic acid hydrates showed a small diversion from Gaussian behavior (beat signal) in the final stage of relaxation, suggesting Abragam-type relaxation.[13] However, T_2 was calculated according to Eq. (1) for the purpose of comparison among API hydrates. The FID signals that show both Gaussian and Lorentzian decay patterns were fitted to Eq. (2) representing the summation of the Gaussian and Lorentzian equations.

$$I(t) = I_0 \exp\left[-\left(\frac{t}{T_2}\right)^2\right] \tag{1}$$

$$I(t) = I_0\left[P_G \exp\left(-\left(\frac{t}{T_{2(G)}}\right)^2\right) + P_L \exp\left(-\frac{t}{T_{2(L)}}\right)\right] \tag{2}$$

where $I(t)$ and I_0 are signal intensity at time t and time 0. $T_{2(G)}$ and $T_{2(L)}$ are T_2 for Gaussian decay and Lorentzian decay, respectively, and P_G and P_L are the proportion of protons that show Gaussian decay and Lorentzian decay, respectively.

The T_1 of proton in API hydrates was determined at 30°C by the inversion recovery method. T_1 was calculated according to Eq. (3).

$$I(t) = I_0\left(1 - 2\exp\left(-\frac{t}{T_1}\right)\right) \tag{3}$$

DOI 10.1002/jps

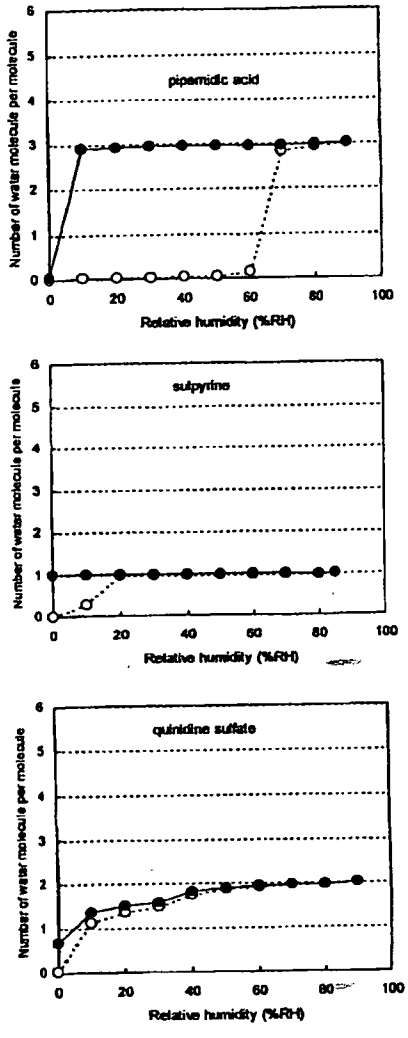

Figure 7. Water sorption isotherms for API hydrates showing a single endothermic peak in DSC thermogram.

Differential Scanning Calorimetry (DSC)

Modulated temperature DSC experiments were performed using a commercial system (2920; TA Instruments[Q6], DE) attached to a refrigerated cooling accessory. The conditions were as follows: modulation period of 100 s, a modulation amplitude of ±0.5°C, and an underlying heating rate of 1°C/min. Temperature calibration was performed using indium. Samples (approximately 10 mg) were put in a pan without a lid. Nitrogen gas was flowed at 30 mL/min.

Water Sorption Isotherm

Water sorption isotherms were measured gravimetrically at 25°C using the automated sorption analyzer from VTI Corp[Q7]. (FL). Prior to water sorption and desorption, samples were dried at 60°C and reduced pressure, until the partial vapor pressure became less than 0.0. Equilibrium water content was measured at ascending partial vapor pressures ranging from 0.10 to 0.95, then at descending partial vapor pressures ranging from 0.95 to 0.00 in steps of 0.10 or 0.05. Equilibrium was regarded to have been achieved once the change in sample weight was less than 0.001 mg over 10 min. The limit duration for measurement at a partial vapor pressure was 10 h for scopolamine hydrobromide and 5 h for the others.

RESULTS

NMR Relaxation Times

Figures 1 and 2 show representative examples of the time courses of spin–spin relaxation observed for the 11 API hydrates. Of the four antibiotic hydrates, all exhibited both Gaussian-type decay and Lorentzian decay, as exemplified by ceftazidime and cefazolin sodium hydrates (Fig. 1). The other seven API hydrates exhibited only Gaussian-type decay, as exemplified by quinidine sulfate and scopolamine hydrobromide hydrates (Fig. 2).

In order to calculate the proportion of water protons to API protons, which is required to obtain the T_2 of the water protons by curve-fitting of decay patterns, the number of water molecules per API hydrate molecule was measured by the Karl Fischer method. The results are shown in Table 1, in which the values specified in the JP are also noted for the purpose of comparison. The measured water contents were consistent with those specified in the JP for pipemidic acid, sulpyrine, and quinidine sulfate hydrates, as well as all antibiotic hydrates except for cefazolin sodium hydrate. In contrast, quinine hydrochloride, scopolamine hydrobromide, and saccharin sodium hydrates showed smaller water contents than those specified in the JP.

The time courses of spin–spin relaxation showing both Gaussian decay and Lorentzian decay observed for the four antibiotic hydrates were well fitted to Eq. (2) using the proportion of water protons calculated from the measured water

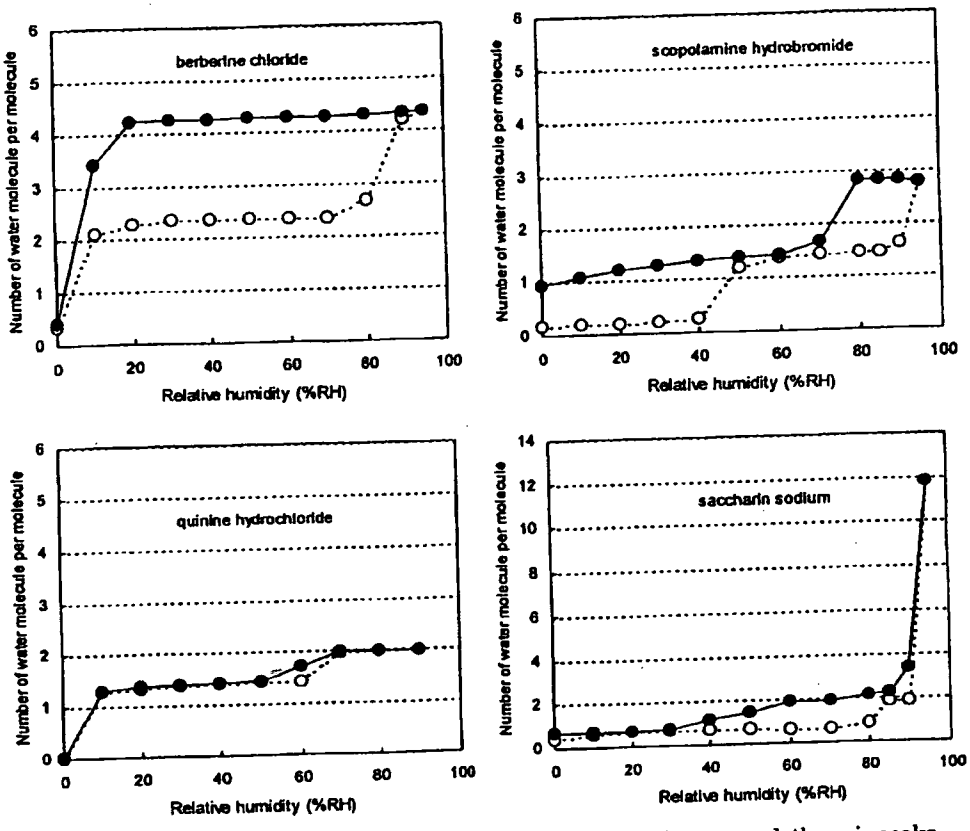

Figure 8. Water sorption isotherms for API hydrates showing two endothermic peaks in DSC thermogram.

content, as shown by the regression curve in Figure 1. Therefore, all of the water protons in the molecule are considered to show Lorentzian decay, and the Gaussian decay is attributed to the drug protons. The T_2 of the Lorentzian decay was calculated according to Eq. (2), and the results will be discussed below. For cefazolin sodium hydrate, better curve-fitting was obtained by regression analysis using a slightly larger value for the proportion of water protons than that calculated from the measured water content. This suggests that a small number of the drug protons exhibit Lorentzian decay; however, it is possible that the water content of the sample used for NMR measurement was different from that of the sample used for Karl Fischer measurements.

The seven API hydrates other than the antibiotic hydrates did not exhibit Lorentzian decay, indicating that all water protons and drug protons in the molecule showed Gaussian decay. The T_2 of the water protons was calculated according to Eq. (1), assuming that the T_2 of the drug protons is similar to that of the water protons. The results will be discussed below.

DSC Thermograms

Figures 3–5 show DSC thermograms measured for the 11 API hydrates. The four antibiotic hydrates, which exhibited Lorentzian decay upon spin–spin relaxation, showed a single endothermic peak due to water evaporation, as shown in Figure 3. In contrast, the API hydrates that did not exhibit Lorentzian decay showed two endothermic peaks (Fig. 4), or one peak (Fig. 5).

The temperature at which an endothermic peak due to water evaporation is observed may be considered to represent the ease of evaporation of hydration water under nonisothermal conditions. The onset temperature was determined as a parameter for approximate comparison of ease of evaporation among the API hydrates, along with ease of evaporation under isothermal conditions as

DOI 10.1002/jps

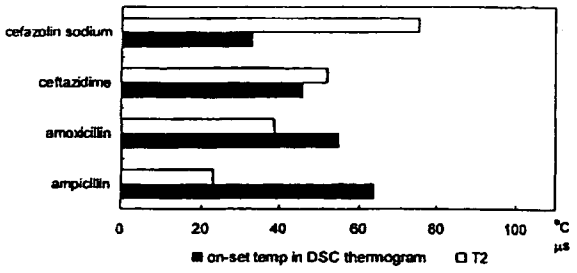

Figure 9. Correlation between onset temperature and T_2 for four antibiotic hydrates.

determined by water vapor sorption analysis. Onset temperature is known to depend on various factors, such as the heating rate, the shapes of the pan and lid, the surface area of the sample, and the flow rate of nitrogen gas. In this study, controllable factors such as the heating rate and the flow rate of nitrogen gas were kept constant, and a pan without a lid was used. The onset temperatures obtained will be discussed below.

Water Vapor Sorption Isotherm

Figures 6–8 show water sorption isotherms observed for the four antibiotic hydrates, the other three API hydrates that exhibited a single endothermic peak due to water evaporation, and the four API hydrates that exhibited two peaks due to water evaporation, respectively. The y-axis represents the number of water molecules per API hydrate molecule, calculated from the water content measured by the Karl Fischer method, assuming that all water molecules present in the sample were evaporated during the drying process (60°C, reduced pressure) prior to the sorption and desorption processes.

The water sorption isotherms (Fig. 6) observed for the four antibiotic hydrates, which exhibited Lorentzian decay upon spin–spin relaxation, indicate that during the desorption process, the water content decreased with decreasing humidity in the range 90–0% RH, with a significant slope in the water content versus humidity plot.

Among the three API hydrates that did not exhibit Lorentzian decay and showed a single endothermic peak due to water evaporation, pipemidic acid and sulpyrine hydrates gave water desorption isotherms in which the water content was constant over a wide humidity range, as shown in Figure 7. Quinidine sulfate also showed a flat line in the water content versus humidity plot, though it was observed only at high humidities.

The water desorption isotherms observed for the other four API hydrates (except berberine chloride), which did not exhibit Lorentzian decay and showed two endothermic peaks due to water evaporation, indicated that the water content remained approximately constant at two levels (Fig. 8).

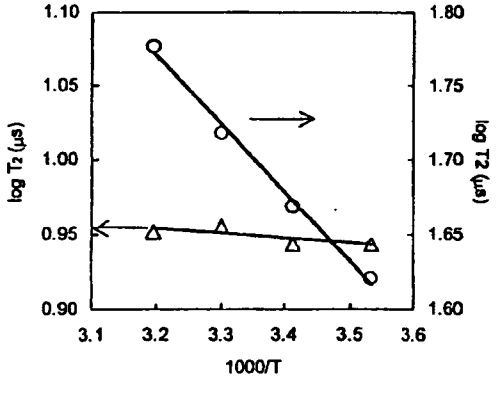

Figure 10. Temperature dependence of T_2 for ceftazidime (circle) and pipemidic acid (triangle) hydrates.

DISCUSSION

The molecular mobility of hydration water in API hydrates was found to vary over a wide range; some, such as ceftazidime hydrate, contain hydration water that shows Lorentzian decay upon spin–spin relaxation, while others contain hydration water that shows Gaussian decay.

Hydration Water Showing Lorentzian Decay

All of the water molecules present in the four antibiotic hydrates were found to exhibit Lorentzian decay, because the proportion of Lorentzian decay was consistent with the proportion of water protons calculated from the water content measured by the Karl Fischer method (Fig. 1). The finding that the water molecules in the antibiotic hydrates showed Lorentzian decay rather than Gaussian decay suggests that water molecules are held in voids in the crystal, rather than being firmly trapped in the crystal lattice. These water molecules may evaporate through channels formed in the interior of the crystal.[14] Hydration water that requires more energy to be released

may exhibit a higher onset temperature of the endothermic peak due to water evaporation in DSC.

The T_2 values determined based on Lorentzian decay is related with τ_c by Eq. (4), such that a smaller value of T_2 represents a larger τ_c (lower mobility).

$$\frac{1}{T_2} = \frac{\gamma^4 \hbar^2 I(I+1)}{5r^6}\left(3\tau_c + \frac{5\tau_c}{1+\omega_0^2\tau_c^2} + \frac{2\tau_c}{1+4\omega_0^2\tau_c^2}\right) \quad (4)$$

where γ, ω_0, I, r, and $\hbar$ are the gyromagnetic ratio, resonance frequency, spin quantum number, spin distance, and the Plank's constant divided by 2π.

As shown in Figure 9, T_2 increased as the onset temperature (Fig. 3) decreased, indicating that hydration water which evaporates at lower temperatures has greater molecular mobility as determined by T_2. This correlation between T_2 and the ease of evaporation under nonisothermal conditions may be explained by assuming that hydration water with a greater T_2 (higher mobility) can escape through channels at a lower temperature.

In order to gain further insight into the correlation between ease of evaporation and the molecular mobility of the hydration water, the ease of evaporation under isothermal conditions was evaluated by water sorption isotherm measurement. Each of the four antibiotic hydrates exhibited a desorption isotherm showing decreases in water content associated with decreases in humidity (Fig. 6). As discussed below, the crystal form of ampicillin hydrate appeared to be altered during the drying process prior to the measurement of water sorption isotherms. Therefore, the isotherm obtained for ampicillin could not be compared with the NMR and DSC data. However, such detrimental effect of predrying was not observed for the other three antibiotic hydrates. The negative water content observed after the desorption process for ceftazidime may be due to chemical degradation occurred under high-humidity conditions or incomplete evaporation of hydration water during predrying. Compared to amoxicillin hydrate, cefazolin sodium hydrate, which has a larger T_2 value, exhibited a greater slope in its water content versus humidity plot. Furthermore, cefazolin sodium exhibited rapid dehydration when humidity was decreased below 20% RH, whereas amoxicillin did not exhibit rapid dehydration until humidity was decreased below 10% RH. These findings suggest that the ease of evaporation of hydration water under isothermal conditions is correlated with molecular mobility as determined by T_2, which supports the conclusion obtained based on DSC measurement. For ampicillin, the slope of the water content versus humidity plot was greater than that of amoxicillin hydrate despite its lower molecular mobility as determined by T_2 and higher onset temperature. This suggests that the drying conditions prior to the sorption and desorption processes were inadequate, which may result in destruction of the crystalline structure. Thus, the isotherm obtained for ampicillin could not be compared with the NMR and DSC data.

As exemplified by ceftazidime hydrate (Fig. 10), T_2 increased significantly with increasing temperature, indicating that T_2 reflects the increases in molecular mobility associated with increases in temperature. Thus, molecular mobility can be considered to correlate with T_2. As shown in Figure 11, antibiotic hydrates with smaller T_2

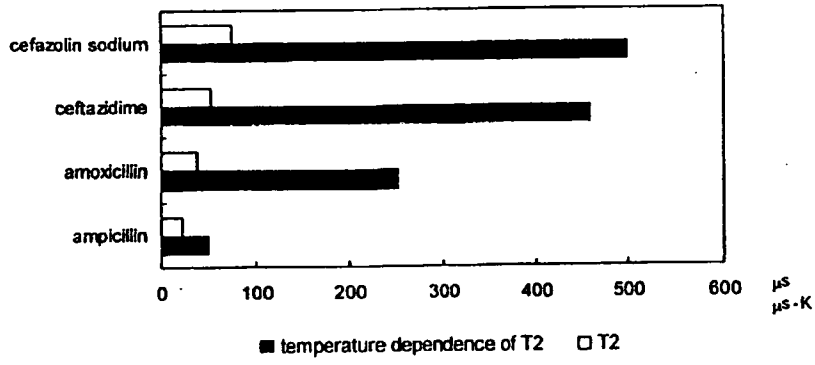

Figure 11. Correlation between T_2 and temperature dependence of T_2 for four antibiotic hydrates.

DOI 10.1002/jps

values showed a smaller change in T_2 with temperature change. This finding suggests that lower values of T_2 reflect a smaller scale of molecular motion, with lower activation energies.

Spin–lattice relaxation time (T_1) is known to reflect molecular mobility, similarly to T_2, but increases with decreasing T_2 (with decreasing molecular mobility) in the slow motional regime. The T_1 values of water protons in the presence of drug protons cannot be determined due to spin diffusion, but an approximate determination of T_1 for water protons is possible if the proportion of water protons is large. For example, in $Na_2HPO_4 \cdot 12H_2O$ and $Na_2HPO_4 \cdot 2H_2O$, water protons are predominant (24/25 and 4/5, respectively). $Na_2HPO_4 \cdot 12H_2O$ exhibits slower spin–spin relaxation (larger T_2) (Fig. 12), and faster spin–lattice relaxation (smaller T_1) (Fig. 13) compared to $Na_2HPO_4 \cdot 2H_2O$, which indicates that both T_1 and T_2 reflect the molecular mobility of hydration water. For the antibiotic hydrates examined, however, correlations between T_1 and T_2 were not observed, as shown in Figure 14. This finding indicates that for API hydrates containing a significant amount of drug protons, such as antibiotic hydrates, the molecular mobility of the hydration water is not reflected in T_1.

Hydration Water Showing Gaussian Decay

As mentioned previously, all of the API hydrates other than the four antibiotic hydrates exhibited only Gaussian decay (Fig. 2). The value of T_2 did not vary significantly among the API hydrates, as shown in Figure 15. Furthermore, the onset temperatures of the single endothermic peaks

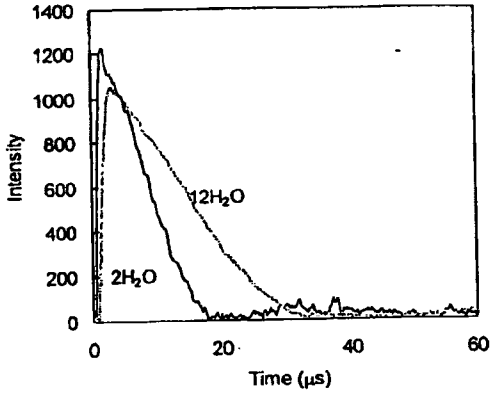

Figure 12. Free induction decay for Na_2HPO_4 $12H_2O$ and $2H_2O$.

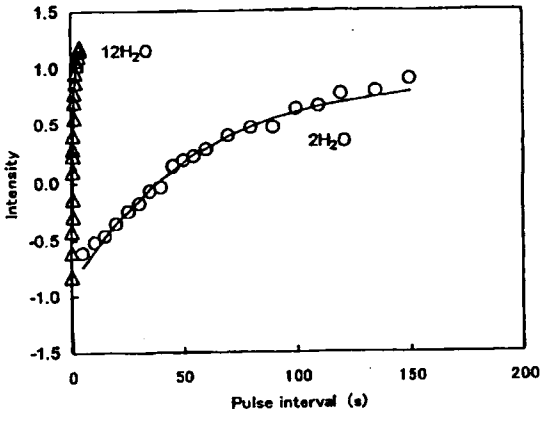

Figure 13. Spin–lattice relaxation for Na_2HPO_4 $12H_2O$ and $2H_2O$.

due to water evaporation for quinidine sulfate, pipemidic acid, and sulpyrine hydrates (Fig. 5), as well as each of the two peaks due to water evaporation observed for quinine hydrochloride, scopolamine hydrobromide, saccharin sodium, and berberine chloride hydrates (Fig. 4), were not correlated with T_2. These findings indicate that the molecular mobility of hydration water that shows Gaussian decay is too low to be reflected in T_2. No correlation between T_2 and molecular mobility is supported by the finding that changes in T_2 associated with changes in temperature were much smaller than those observed for the antibiotic hydrates that exhibited Lorentzian decay, as exemplified by pipemidic acid (Fig. 10). Such low molecular mobility may be attributed to water molecules firmly trapped in the crystal lattice, rather than water molecules trapped in voids in the crystal.

For quinidine sulfate, pipemidic acid, and sulpyrine hydrates, a single endothermic peak was observed in DSC (Fig. 5). The water content versus humidity plots showed a flat line at a certain number of water molecules. Pipemidic acid and sulpyrine showed a flat line at three and one water molecule(s) per hydrate, respectively, and evaporation of these water molecules was observed only under very low humidity (Fig. 7). These findings indicate that water molecules are firmly trapped in the crystal.

For quinine hydrochloride, scopolamine hydrobromide, saccharin sodium, and berberine chloride hydrates, two endothermic peaks were shown in DSC (Fig. 4). The water content versus humidity plots for these hydrates (except for berberine chloride) showed flat lines at two levels

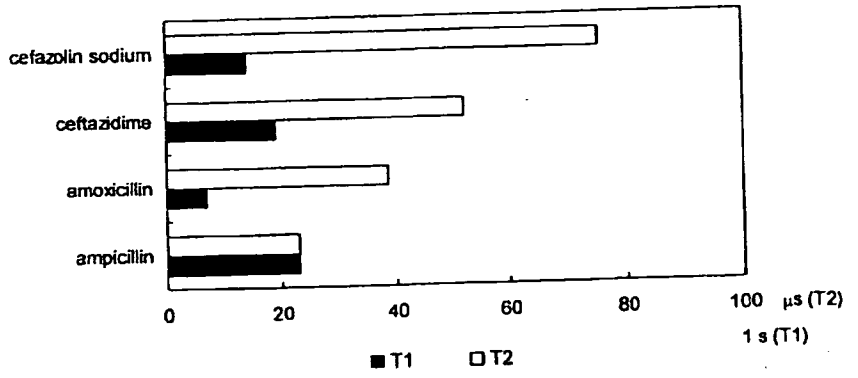

Figure 14. Correlation between T_1 and T_2 for four antibiotic hydrates.

of water content (Fig. 8), suggesting the presence of two water populations: molecules that evaporate at high humidity, and others that evaporate at lower humidity (below 10% RH). This seems to be consistent with the observation of two endothermic peaks in DSC. The endothermic peak observed at a high temperature and the flat line observed at a low humidity may be attributable to hydration water with strong hydrogen–bonding interactions, while the one observed at a lower temperature and higher humidity may be attributable to hydration water with week interactions. The presence of hydration water with week interactions is also supported by the finding that the water contents as measured by the Karl Fischer method were smaller than those specified in the JP (Tab. 1).

CONCLUSION

It was found that spin–spin relaxation time, T_2, is a useful parameter that can indicate the molecular mobility of water of hydration which has relatively high mobility and shows Lorentzian decay upon spin–spin relaxation. For these water molecules, molecular mobility as determined by T_2 is correlated with ease of evaporation both under nonisothermal and isothermal conditions,

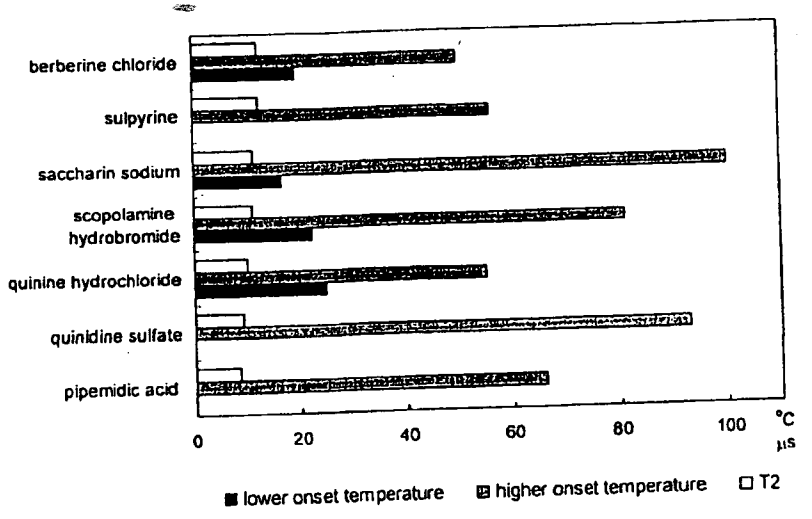

Figure 15. Correlation between onset temperature and T_2 for API hydrates that show Gaussian decay.

DOI 10.1002/jps

such that water molecules with greater ease of evaporation have higher T_2 values.

In contrast, for hydration water that has low mobility and shows Gaussian decay, T_2 was found not to correlate with ease of evaporation under nonisothermal conditions, suggesting that molecular motion that determines the ease of evaporation is not reflected in T_2; in this case, T_2 cannot be used as a parameter to indicate molecular mobility.

The water molecules in the API hydrates studied were found to have wide-ranging molecular mobilities, from low molecular mobility that could not be evaluated by NMR relaxation times, such as the water molecules in pipemidic acid hydrate, to high molecular mobility that could be evaluated by NMR relaxation times, such as the water molecules in ceftazidime hydrate.

REFERENCES

1. Yoshioka S, Aso Y. 2007. Correlations between molecular mobility and chemical stability during storage of amorphous pharmaceuticals. J Pharm Sci 96:960–981.
2. Ahlneck C, Zografi G. 1990. The molecular basis for moisture effects on the physical and chemical stability of drugs in the solid state. Int J Pharm 62:87–95.
3. Mimura H, Gato K, Kitamura S, Kitagawa T, Kohda S. 2002. Effect of water content on the solid-state stability in two isomorphic clathrates of cephalosporin: Cefazolin sodium pentahydrte (α form) and KF041 hydrate. Chem Pharm Bull 50:766–770.
4. Zografi G. 1988. States of water associated with solids. Drug Dev Ind Pharm 14:1905–1926.
5. Newman AW, Reutzel-Edens SM, Zografi G. 2007. Characterization of the "hygroscopic" properties of active pharmaceutical ingredients. J Pharm[Q8] Sci.
6. Brittain HG, Grant DJW. 1999. Effect of polymorphism and solid state solvation on solubility and dissolution rate. In: Polymorphism[Q9] in pharmaceutical solids. New York: Marcel Dekker. pp 279–330.
7. Shinyashiki N, Asaka N, Mashimo S. 1990. Dielectric study on dynamics of water in polymer matrix using a frequency range 10^6–10^{10} Hz. J Chem Phys 93:760–764.
8. Ahlqvist MU, Taylor LS. 2002. Water dynamics in channel hydrates investigated using H/D exchange. Int J Pharm 241:253–261.
9. Ruan R, Chen PL. 1998. Mobility of water in food and biological systems. In: Water in foods and biological materials, a nuclear magnetic resonance approach. ???[Q10]: Technomic Publishing Company, Inc. pp 149–228.
10. Oksanen CA, Zografi G. 1993. Molecular mobility in mixtures of absorbed water and solid poly(vinylpyrrolidone). Pharm Res 10:791–799.
11. Otsuka T, Yoshioka S, Aso Y, Kojima S. 1995. Water mobility in aqueous solutions of macromolecular pharmaceutical excipients measured by oxygen-17 nuclear magnetic resonance. Chem Pharm Bull 43:1221–1223.
12. Mansfield P. 1965. Multiple-pulse nuclear magnetic resonance transients in solids. Phys Rev 137:A961–A974.
13. Parizel N, Meyer G, Weill G. 1993. Nuclear magnetic resonance linesahape studies of interpenetrating polymer networks. Polymer 12:2495–2502.
14. Morris KR. 1999. Structural aspects of hydrates and solvates. In: Polymorphism[Q11] in pharmaceutical solids. New York: Marcel Dekker. pp 125–181.

Q1: Author: Please check the suitability of the suggested short title.
Q2: Author: Please provide complete location.
Q3: Author: Please provide complete location.
Q4: Author: Please provide complete location.
Q5: Author: Please check the country name.
Q6: Author: Please provide the city name.
Q7: Author: Please provide the city name.
Q8: Author: Please provide the volume number and page range.
Q9: Author: Please provide the editors name.
Q10: Author: Please provide the editors name and publisher location.
Q11: Author: Please provide the editors name.

Online Jul. 13
(a)
Lancaster, Pa
Brittain HG (ed)
Brittain HG (ed)
no editor.

日薬理誌（*Folia Pharmacol. Jpn.*）**131**，102～108（2008）

総説

抗体医薬の現状と展望

川西　徹

要約：抗体医薬は今現在最も活発に開発が行われている医薬品群の一つである．その背景としては，(1)異種タンパク質としての抗原性の壁を乗り越えるキメラ抗体あるいはヒト化抗体，ヒト抗体製造技術の完成，(2)ゲノム創薬による医薬品開発の標的となる数多くの疾患関連遺伝子および疾患関連タンパク質の解明，の2点があげられる．現在上市されている抗体医薬のほとんどは構造的にはIgGサブクラスであり，薬効からは主に抗腫瘍薬と免疫調節薬に分類されるが，今後は機能的に必要なコンポーネントに小型化した抗体や，細胞表面の受容体等と結合し細胞内情報伝達を引き起こすアゴニスト抗体，あるいは分子標的薬のコンポーネントとしての利用等，抗体医薬の利用は拡大してゆくことが予想される．しかしながら，これら次世代抗体医薬の開発にあたっては，薬理作用の解析，あるいは安全性予測という面で種差の壁があり，化学合成医薬品で通常用いられる齧歯類動物を主体とした非臨床試験による評価には限界がある．したがって，ヒト初回投与前の安全性予測においては，適切なインビトロ試験系の構築，適切な動物を用いたインビボ試験，さらにはトランスジェニック動物や相同タンパク質等を利用した試験等を組み合わせた試験による解析が必要であり，薬理学者の智恵と経験が必要とされる．

1.　はじめに

現在大学学部用の薬理学教科書を眺めてみると，タンパク質性高分子医薬品に関する記述は極めて限られたものであり，1000ページ弱の標準的教科書でみれば，占める割合は10ページにも満たないものがほとんどである．さらにその対象を抗体医薬に絞ると，抗腫瘍薬あるいは免疫調節薬の項の末尾に小さく扱われているだけで，多いものでも，あわせて2ページにも満たない．しかし眼を新薬開発の世界に転じると，今現在最も注目されている医薬品群の一つは抗体医薬であり，さらには従来の化学合成医薬品では治療が困難であった疾病治療の標準的治療薬の地位を確立しつつある抗体医薬も出現しており，近い将来，薬物治療の教科書の書き換えは必至の状況である．そこで，本稿では，このような抗体医薬開発ブームがおこった背景，代表的な抗体医薬を概説するとともに，今後現れることが予想される抗体医薬，さらには抗体医薬開発の今後の課題，および課題解決において薬理学の果たすべき役割について概説したい．

2.　今なぜ抗体医薬か？

21世紀初頭の現在，最も活発に開発が行われ，欧米を中心として新薬申請が活発な医薬品群の一つは抗体医薬である．振り返れば，抗体医薬開発ブームは1980年代に一度おこっている．その契機はKohler and Milsteinによるハイブリドーマを利用したモノクローナル抗体作製技術の確立にあった(1)．この技術によって，抗原に選択的に結合する抗体の効率的な生産が可能となり，癌治療への応用等が試みられた．しかしハイブリドーマモノクローナル抗体は，通常マウス由来の免疫グロブリンでありヒトに対しては異種タンパク質であるため抗原性が強く，ヒト体内で作られる中和抗体による作用の減弱，あるいはアナフィラキシーショックのため，医薬品としての利用は限定されたものとなった．

一方，現在の抗体医薬開発ブームは以下の2つを理由として生じたといえる．第一に組換えタンパク質作製技術，あるいはトランスジェニック動物作製技術等のバイオテクノロジーの飛躍的進歩により，キメラ抗体，ヒト化抗体等の遺伝子工学利用抗体の作製が可能

キーワード：抗体医薬，バイオテクノロジー応用医薬品，抗腫瘍薬，免疫調節薬
国立医薬品食品衛生研究所薬品部（〒158-8501 東京都世田谷区上用賀1-18-1）
e-mail: kawanish@nihs.go.jp　原稿受領日：2007年10月10日，依頼原稿
Title: Antibody drugs: the present status and perspectives.　Author: Toru Kawanishi

となったことである(2, 3)．これらの技術によって，従来のモノクローナル抗体が異種タンパク質であるゆえに生じた問題を回避できるようになった．

抗体医薬開発ブームが起こった第二の理由は，ゲノム創薬の本格化があげられる．ゲノム創薬は，生体の遺伝子あるいはタンパク質の構造，機能情報をもとに，医薬品シーズを発見，設計する医薬品開発手法であるが，今現在は疾病関連遺伝子あるいは疾病関連タンパク質の発見／特定，さらには疾病に至るメカニズムの解明は相次いでいるものの，これらの情報をもとに疾病治療用医薬品を効率的にデザインする手法の完成にまでは至っていない．その点で，疾病関連タンパク質に選択的に結合する抗体を生体の免疫系を利用して作製し，選別することにより最適の医薬品シーズを発見する手法は，様々な疾患関連タンパク質に対して共通に応用できる技術である．また，現在抗体医薬の開発に多くの企業が注力している理由としては，このような抗体医薬の開発の成功率の高さがあげられ，実際米国において第Ⅰ相臨床試験が実施されたもののうち上市に至った割合は低分子化合物では約5%であるのに対し，抗体医薬では約20%という報告もある(4)．

3. 遺伝子工学利用抗体の作製法

キメラ抗体とは遺伝子組換え技術を用いてマウスモノクローナル抗体の定常 constant（C）領域をヒト抗体のC領域に置き換えた抗体である．一方ヒト化抗体は抗体タンパク質の三次元構造をもとに，抗原に結合する相補性決定領域 complementarity determining region（CDR）の1から3を残して，それ以外の部分である抗体のフレーム領域 frame region（FR）を全てヒト抗体に置き換えたものである（図1）．以下に，マウスハイブリドーマ細胞から遺伝子組換え法によるキメラ抗体，ヒト化抗体の作製法を紹介する．

キメラ抗体作成の第一ステップは，マウス抗体産生ハイブリドーマからのマウス抗体をコードする遺伝子のクローニングである．通常ハイブリドーマ細胞よりRNAを抽出し，cDNAを作製後，プラークハイブリダイゼーション法あるいはPCR法により抗体遺伝子をクローニングする方法，あるいはRNAより直接PCR法により抗体遺伝子をクローニングする方法が用いられている．次にクローニングしたマウス抗体の可変（V）領域遺伝子にヒトのC領域遺伝子を連結し，適当な発現ベクターに挿入して培養細胞で生産する．また，抗体産生ハイブリドーマのマウス抗体C領域をヒト抗体C領域に組み換える相同組換え法やトランスジェニックマウスによっても作成される．

ヒト化抗体遺伝子の作製はさらに複雑なステップである．第一ステップではクローニングしたマウス抗体V領域における抗原との結合に寄与するCDR配列とヒト抗体V領域におけるアイソタイプ固有のアミノ酸配列をもつフレームワーク領域（FR）から成るV領域をコードする遺伝子を構築する．これにヒトのC領域遺伝子を連結し，構築された抗体 heavy（H）鎖および light（L）鎖遺伝子が挿入された発現ベクターを製造用動物細胞に導入し，遺伝子組換え抗体を発現する．製造細胞としては，チャイニーズハムスター卵巣由来のCHO細胞，マウスミエローマ由来のNS0細胞およびSP2/0細胞等が用いられることが多い(5)．

このようにヒト化抗体は高度な遺伝子組換え技術を利用して製造されるが，CDR配列部分はマウス由来である．そこですべてヒト由来の完全ヒト抗体の作成法が開発された．主な方法としては2種類あり，一つはファージディスプレイ法，一つはヒト抗体作製用トランスジェニックマウス法である．前者のファージディスプレイ法は大腸菌ウイルスの一つであるM13やT7などの繊維状ファージのコートタンパク質（g3p

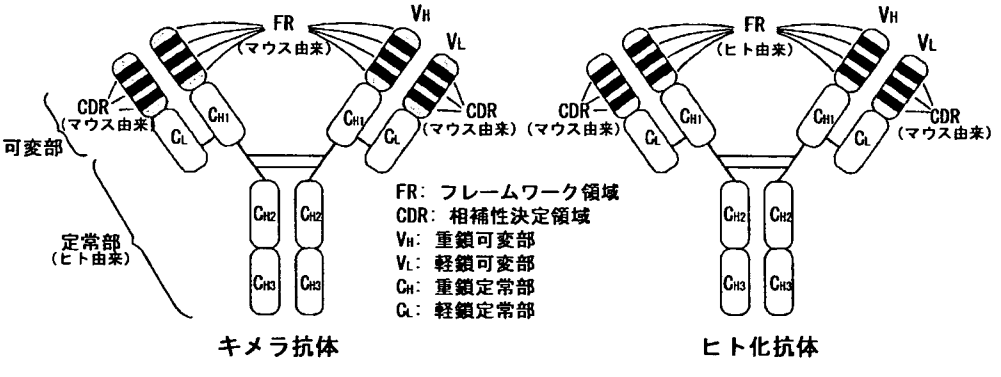

図1　キメラ抗体およびヒト化抗体の構造

表1 日米欧における既承認抗体医薬一覧[1)]

名称	商品名	種類	標的	主な適応疾患	承認をうけた年度 米国	欧州	日本	抗体生成頻度[2)]
抗腫瘍薬								
Rituximab	Rituxan, MabThera	キメラ抗 IgG1κ	CD20	B細胞性非ホジキンリンパ腫	1997	1998	2001	<1%
Trastuzumab	Herceptin	ヒト化抗体 IgG1κ	HER2	転移性乳ガン	1998	2000	2001	0.1%
Denileukin Diftitox	Ontak	融合タンパク質 IL2 + Diphtheria toxin	IL2R	皮膚T細胞リンパ腫	1999	NA[3)]	NA	8%
Gemtuzumab ozogamicin	Mylotarg	ヒト化抗体 IgG4κ（カリケアマイシン結合）	CD33	急性骨髄性白血球	2000	NA	2005	
Alemtuzumab	Campath, MabCampath	ヒト化抗体 IgGaκ	CD52	B細胞性慢性リンパ性白血病	2001	2001	NA	<2%
Ibritumomab tiuxetan	Zevalin	マウス抗体 IgG1κ (^{90}Y標識)	CD20	B細胞性非ホジキンリンパ腫	2002	2004	NANA	
Iodine 131 Tositumomab	Bexxar	マウス抗体 IgG2aλ (^{131}I標識)	CD20	非ホジキンリンパ腫	2003	NA	NA	
Cetuximab	Erbitux	キメラ抗体 IgG1κ	EGFR	頭頸部癌，結腸・直腸癌	2004	2004	NA	5%
Bevacizumab	Avastin	ヒト化抗体 IgG1	VEGF	結腸・直腸癌	2004	2005	2007	ND
Panitumumab	Vectibix	ヒト化抗体 IgG2κ	EGFR	結腸・直腸癌	2006	NA	NA	
免疫調節薬								
Muromonab-CD3	Orthoclone OKT3	マウス抗体 IgG2a	CD3	腎移植後の急性拒絶反応	1986	NA	1991	~80%
Daclizumab	Zenapax	ヒト化抗体 IgG1κ	CD25	腎移植後の急性拒絶反応	1997	1999	NA	
Basiliximab	Simulect	キメラ抗体 IgG1κ	CD25	腎移植後の急性拒絶反応	1998	1998	2002	<2%
Infliximab	Remicade	キメラ抗体 IgG1κ	TNFα	関節リウマチ	1998	1999	2002	10-57%
Etanercept	Enbrel	融合タンパク質 TNFαR + Fc	TNFα	関節リウマチ関節リウマチ	1998	2000	2005	
Adalimumab	Humira	ヒト抗体 IgG1κ	TNFα	関節リウマチ	1998	2002	2003	NA
Efalizumab	Raptiva	ヒト化抗体 IgG1κ	CD11	尋常性乾癬	2003	2004	NA	
Omalizumab	Xolair	ヒト化抗体 IgG1κ	IgE	喘息	2003	2003	2005	NA
Alefacept	Amevive	融合タンパク質 LFA3 + Fc	CD2	尋常性乾癬	2003	NA	NA	
Natalizumab	Tysabri	ヒト化抗体 IgG4κ	α4integrin	多発性硬化症	2004	2006	NA	
Abatacept	Orencia	融合タンパク質 CTLA4 + Fc	CD80/CD86	関節リウマチ	2005	NA	NA	
Tocilizumab	Actemra	ヒト化抗体 IgG1κ	IL6R	キャッスルマン病	NA	NA	2005	
Eculizumab	Soliris	ヒト化抗体 IgG2/4κ	C5a	発作性夜間血色素尿症	2007	2007	NA	
その他								
Abciximab	ReoPro	キメラ抗体 IgG1（Fab）	GPIIb/IIIa	心筋虚血	1994	NA	NA	7-19%
Palivizumab	Synagis	ヒト化抗体 IgG1κ	RSVFProtein	RSウィルス感染	1998	1999	2002	<1%
Ranibizumab	Lucentis	ヒト化抗体 IgG1κ（48Kフラグメント）	VEGF-A	加齢黄斑変性	2006	2007	NA	

1）文献9より改変，2）文献10中の値，3）NA：未承認

やg10pなど）のN末端側にファージの感染性を失わないよう外来遺伝子を融合タンパク質として発現させるシステムである．一度に10^8種類以上ともいわれる多種類の分子種を呈示したライブラリーを構築でき，また粒子ごとに目的の機能や性質をもった分子種を選択できる．この技術を用いて外来遺伝子として抗体の結合部位である2つのポリペプチド鎖VHとVLを短いリンカーで直列につないだ単鎖Fv single-chain Fv (scFv) をファージにディスプレイさせたものが抗体ファージライブラリーである．そしてファージライブラリーから特異的抗体ファージをスクリーニングする．これを最終的にファージから切り離したものがファージディスプレイ抗体である(6, 7)．

完全ヒトモノクローナル抗体取得のもう一つの方法は，ヒト抗体を産生するトランスジェニック動物の利用である．内因性Igをノックアウトしたマウスに機能的なヒトのIg遺伝子を導入すれば，マウス抗体の代わりに多様な抗原結合能を持つヒト抗体が産生されると考えられる．さらにこのマウスを免疫すればヒトモノクローナル抗体を従来のハイブリドーマ法で得ることが可能である．既にKMマウス，KWマウス，HACマウス等のヒト抗体産生用マウスが開発され，完全ヒト抗体の製造に利用されている(8)．

4. 遺伝子工学利用抗体医薬の利点

2. においてキメラ抗体，ヒト化抗体，ヒト抗体の利点として，異種タンパク質ゆえの抗原性の克服について言及したが，表1に日米欧で認可をうけている抗体医薬に対するヒトでの抗体の検出頻度を記した．この数字から明らかなように，ハイブリドーマ抗体医薬では，極めて高い頻度の抗体医薬に対する抗体の出現が報告されている．一方，キメラ抗体においてはフレームワークを含む可変領域が抗原性を残しているため，抗体によって高い抗体生成が報告されている製品はあるものの，ハイブリドーマ抗体に比べれば全般的に抗体生成頻度は低い．ヒト化抗体は，理論的には抗原性を示す部位はマウス由来のCDR配列のみであり，比較的低い数字が報告されている(10)．

このような中和抗体の生成とも関連することであるが，ハイブリドーマ抗体については，ヒト抗体と比較してヒト血中半減期が極めて短いことが指摘されてきた（ヒト抗体：23日，ハイブリドーマ抗体：1-3日）．また，組換えキメラ抗体，ヒト化抗体においては，ハイブリドーマ抗体に比べると，一般に血中半減期が長いことが報告されている．このメカニズムが最近になって明らかになってきた．即ち，母親から胎児に液性免疫を伝える機構を担うIgG胎児性Fc受容体(FcRn)は，成長後も免疫グロブリンの体内循環を担うことにより血中半減期の延長に役だっていること，さらには疾病治療用抗体医薬の血中半減期の改善に，IgGのFc領域とFcRnとの相互作用が利用できることが明らかにされている(11, 12)．

5. 既に上市されている主な抗体医薬

現在までに日米欧で認可された抗体医薬を表1にまとめた．対象疾患は様々であるが，大別すると主に抗腫瘍薬，および免疫調節薬に分類される．抗腫瘍薬としてはリツキシマブ，トラスツズマブ，ゲムツズマブオゾガマイシン，ベバシズマブ等は，現在標準的治療に使用される医薬品としての評価を得るまでになっている．また免疫調節薬のなかで，インフリキシマブはメトトレキセートの併用薬として関節リウマチの治療に使用されることが多い．さらにヒト型遺伝子組換え可溶性TNF α受容体-Fc融合タンパク質のエタネルセプトは，IgGではなく抗体のFc領域を利用した人工タンパク質であるが，メトトレキセートとの併用の必要のない関節リウマチ治療薬である．加えて日本発であるヒト化抗IL-6受容体抗体トシリズマブ（中外製薬と大阪大学の共同開発）は，キャッスルマン病治療薬として認可されたが，関節リウマチへの適用拡大を目指した試験で好成績を得たとされている．

このように，多くの抗体医薬が疾病治療に有効であることが示され，新薬として脚光をあびている．

6. 今後開発が予想される次世代抗体医薬

以上のように，抗体医薬は欧米を中心に既に数多くの製品が承認されているが，既承認抗体医薬は融合タンパク質型以外の製品では，いずれも構造的にはIgGのサブクラスに属し，機能的にも構造的にも分離可能な2つのモジュール：1）抗体認識部位であるV領域：2）抗体が抗原に結合した後のCDC（Complement Dependent Cytotoxicity 補体依存性細胞障害：抗体が細胞膜表面上の抗原決定基に特異的に結合して，補体の介助のもとで，その細胞に傷害を与えること）活性あるいはADCC（Antibody Dependent Cell-mediated Cytotoxicity 抗体依存性細胞傷害：IgGクラス抗体のFc領域がT細胞，NK細胞，好中球，マクロファージ上のFc受容体を介して，これらエフェクター細胞を活性化し，抗体の可変領域が結合した細胞を殺すこと）活性等の反応を惹起するエフェクター機能を担うFc領域から構成されている．しかしこのようなIgG抗体医薬の分子量は10万をこえる巨大分子であるた

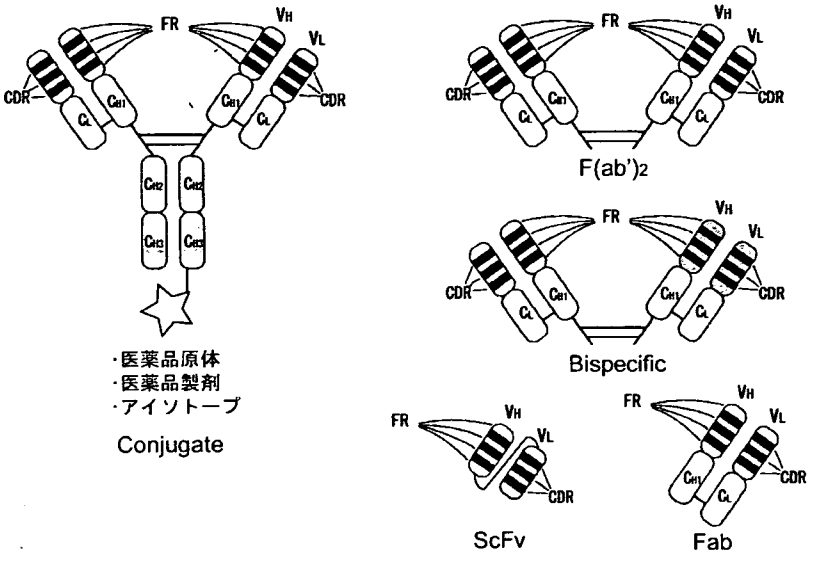

図2 今後出現すると思われる次世代抗体医薬
(文献13より改変)

め，血中から組織への移行はきわめて遅い．その解決策としてファージディスプレイなどの方法を用いたScFvタイプ，あるいはFabタイプ，$F(ab')_2$タイプ等，サイズを小さくし，生体内移行性を増大する抗体医薬の検討が行われている（図2）．さらには，異なる抗原特異性を有する抗体に由来するFabフラグメントをつなぎ，2つの特異性bispecificを有する$F(ab')_2$タイプの医薬品としての利用も試みられている．一方このような低分子化抗体は，既存の化学合成医薬品原体，あるいは医薬品製剤に結合させることにより，これら医薬品に標的性を付与させることが可能となるので，今後分子標的薬開発のコンポーネントとしての利用も活発化することが予想される．

以上のような抗体のアミノ酸配列部分の改変以外に，糖鎖改変抗体の作製も試みられている．既承認の抗体医薬のほとんどはIgG型であり，Fc部分のCH2領域にアスパラギン結合型のコンプレックス型糖鎖を持つ糖タンパク質である．抗体の糖鎖は共通のコア部分に，修飾が異なる30種類以上のオリゴ糖の末端がついた混合物であるが，この糖鎖の付け根に付いているフコースがなくなるとADCC活性が動物レベルで100倍上昇する．したがって，抗体のFc領域に結合している糖鎖からフコース残基を除去すると，高いADCC活性が誘導される(14, 15)．

以上のような，構造的に新しいタイプの抗体医薬とともに，作用機構の上でも新しいタイプの抗体医薬の創製が活発化するものと考えられる．即ち，従来の抗体医薬の多くは疾病関連タンパク質への親和性を利用し，(1)これらタンパク質を中和，(2)酵素や受容体等の反応をブロック，(3)細胞膜の標的タンパク質に結合しFc領域のエフェクター機能による細胞傷害等によって薬理作用を発現する．しかし次世代の抗体医薬としては，細胞表面受容体等（例えばトロンビン受容体，エリスロポエチン受容体，成長ホルモン受容体，FAS，CD20，CD28）に結合し，アゴニストとして細胞内情報伝達を引き起こすことを目指したアゴニスト抗体の開発も精力的に行われている．

7. 次世代抗体医薬の薬理作用の解析および安全性評価

以上のように，抗体医薬開発は広汎かつ活発に行われているが，昨年3月このような抗体医薬の安全性評価法の信頼を揺るがす臨床試験事故が起こった．問題となった医薬品候補化合物はTリンパ球表面のCD28に結合するヒト化モノクローナル抗体TGN1412で，ドイツのTeGenero社によって開発されていた抗CD28アゴニスト抗体（スーパーアゴニスト）であった．従来のモノクローナル抗体では，単独でT細胞を活性化できないが，このスーパーアゴニストは結合部位の違いから単独でT細胞を活性化させ，T細胞の増殖およびサイトカイン産生を誘導することができるとされ，B細胞慢性リンパ球白血病等の血液系の悪性腫瘍や関節リウマチ等の慢性炎症性疾患の治療薬として開発が進められていた(16, 17)．初回臨床試験は0.1

mg/kg の静脈投与で実施されたが，被験者 6 名全員に重度のサイトカイン放出症候群が生じ，多臓器不全に陥った．症状は極めて重篤であったものの，救命処置により幸い死亡には至らなかった(18)．この事故が臨床試験の専門家を混乱に陥れたのは，この薬は欧州規制当局 EMEA によりオーファン薬として指定をうけ，治験申請についても当然のことながら規制当局からの承認をうけていたことである．

事故の原因分析は，英国および欧州規制当局によって詳細に実施されている(19, 20)．まずこの治験に使われたロットについての品質面の詳細な分析の結果，不純物等の品質の問題による事故でないことが明らかにされた．そこで，検討はヒト初回投与試験における投与方法と用量の妥当性を中心に行われた．まず投与方法についてであるが，カニクイザルでの実験が 1 時間をかけた点滴注射で行われたのに対して，ヒト初回投与試験では短時間(1-5 分）の静注を行った点は，サイトカイン放出症候群を招いた原因として充分考えられるポイントである．一方初回臨床試験の投与用量であるが，カニクイザルでの 28 日間反復投与試験結果で，5 mg/kg および 50 mg/kg 投与によりリンパ球の活性化，それを反映した IL-5，IL-6 の上昇がみられたものの，これらの作用は薬理作用と考え，それ以外には特段の有害作用はみられなかったと判断，無毒性量 NOAEL を 50 mg/kg とし，この数字をもとに安全率を 500 倍とって決定したものであり(21)，従来の評価法の基準からすると必ずしも間違いとはいえない．しかし，英国 National Institute of Biological Standards and Control（NIBSC）の報告では，TGN1412 の作用のインビトロ検出系を新たに構築，その解析結果によると，カニクイザルのリンパ球では TGN1412 による細胞増殖やサイトカイン産生は検出されないが，ヒトリンパ球ではどちらも検出できアゴニスト作用が確認できること，しかもその濃度作用曲線はベル型を示し，至適濃度は 2-10 μg/ml であることを見いだしている(22)．この結果は，カニクイザルの実験ではヒトの作用の予測が困難な場合があることを示している．

バイオテクノロジー応用タンパク質性医薬品の安全性評価については，(1)従来の医薬品のほとんどは物質的にも天然のヒトタンパク質に限りなく近いことを目標に設計されている，(2)したがって生理的条件と同様な暴露条件なら，作用は予測可能である，(3)齧歯類動物を中心とした非臨床試験は，種差の壁により薬理作用および毒性の解析は困難な場合が少なくない，(4)試験動物にとって被験物質は異種タンパク質であり，中和抗体の生成等によって正確な作用プロファイルの解析は困難である．したがって，これら医薬品の非臨床安全性試験ガイドライン(23）では，動物を用いる非臨床試験の有用性は化学合成医薬品の場合に比べて限られるとされ，また，ヒト型標的タンパク質を発現させたトランスジェニック動物，あるいは相同タンパク質による検討を推奨している．このガイドラインが運用され，既に 7 年が経過しているが，トランスジェニック動物あるいは相同タンパク質は，未だ推奨の段階に終わっているのが実状である．一方，アゴニスト抗体は天然の生理活性物質とは異なる薬理作用を示すことが期待されて作製されるタンパク質であり，生物学的な実験なしに作用の予測は困難である．また低分子抗体はヒト抗体と同様の特異性を有しているとしても，ヒト抗体では分布しえない体内部位に分布し作用する．したがって，今後これらの新しいタイプの抗体医薬をヒトに投与するにあたっての作用の解析は，適切なインビトロ系の構築，適切な種の動物を用いたインビボ解析，さらに可能な場合は相同タンパク質あるいはトランスジェニック動物等の利用によって，作用機構の解析，濃度作用相関あるいは用量作用相関の解析を行うことが必要である．EU ではすでに，これらハイリスク薬のヒト初回臨床試験において考慮すべき要件をまとめたガイドラインを作成しており，投与量を決定する場合は，最小予測生物学的影響量 Minimal Anticipate Biological Effect Level（MABEL）に基づくこと等の推奨を盛り込んでいる(24)．

8. おわりに

抗体医薬の開発は活発に行われており，近い将来薬理学の教科書にも大幅に取り入れる必要が生じるであろう．さらに今後構造面からも作用機構からも新しいタイプの抗体医薬開発が活発化することが予想される．このような次世代抗体医薬の開発においては薬理作用の解析，および安全性予測のためには，インビボ，インビトロ実験系を駆使した薬理作用の解析が重要であり，その解析には薬理学者の智恵と経験が必要とされる．

謝辞：本総説に関わる研究の一部は，厚生労働省科学研究費補助金医薬品・医療機器レギュラトリーサイエンス総合研究事業に対する助成金によるものである．ここに謝意を表する．

文 献

1) Kohler G, et al. Nature.1975:256:495-497.
2) Morrison SL, et al. Chimeric immunoglobulin genes:Immunoglobulin genes. Academic Press;1989.p.260-278.
3) Roguska MA, et al. Proc Natl Acad Sci USA. 1994;9:969-973.
4) Chapman K, et al.Nature Rev. 2007;6:120-126.
5) Chu L, et al. Curr Opin Biotechnol. 2001;12:180-187.
6) Winter G, et al. Ann Rev Immunol. 1994;12:433-455.
7) Burton DR, et al. Adv Immunol. 1994;57:191-280.
8) 石田 功. 実験医学. 2002;20:846-851.
9) 山口照英, 他. 谷本学校毒性質問箱. 2007;10:~~(印刷中)~~
10) Koren E, et al. Curr Pharm Biotechnol. 2002;3:349-360.
11) Lobo ED, et al. J Pharm Sci. 2004;93:2645-2668.
12) Roopenian DC, et al. Nature Rev. 2007;7:715-725.
13) VanDijk MA, et al. Monoclonal Antibody-Based Pharmaceuticals: Pharmaceutical Biotechnology 2nd Ed. Taylor & Francis;2002. p.283-299.
14) Shinkawa T, et al. J Biol Chem. 2002;278:3466-3473.
15) Shields RL, et al. J Biol Chem. 2002;277:26733-26740.
16) Beyersdorf N, et al. Ann Rheum Dis. 2005;64 Suppl 4：iv91-95.
17) Margulies DH. J Exp Med. 2003;197:949-953.
18) Suntharalingam G, et al. N Engl J Med. 2006;355:1018-1028.
19) Early stage clinical trial taskforce; Joint ABPI/BIA report. [cited; Available from:http://www.abpi.org. uk/information/pdfs/BIAABPI_taskforce2.pdf
20) Expert group on phase one clinical trials: Final report.[cited; Available from: http://www.dh.gov. uk/en/Publicationsandstatistics/Publications/PublicationsPolicyAndGuidance/DH_063117
21) Kenter MJ, et al. Lancet. 2006;368:1387-1391.
22) Stebbings R, et al. J Immunol. 2007;179:3325-3331.
23) バイオテクノロジー応用医薬品の非臨床における安全性評価. [cited; Available from:http://www.pmda.go. jp/ich/s/s6_00_2_22.pdf]
24) Guideline on strategies to identify and mitigate risks for first-in-human clinical trials with investigational medicinal products. [cited;Available from:http://www.emea.europa.eu/pdfs/human/swp/2836707enfin.pdf]

著者プロフィール

川西 徹（かわにし とおる）

国立医薬品食品衛生研究所 薬品部 部長，博士（薬学）．◇1977年東京大学大学院薬学系研究科修士課程修了，同年国立衛生試験所（現国立医薬品食品衛生研究所）安全性生物試験研究センター薬理部研究員（この間，カリフォルニア大学バークレー校，ノースカロライナ大学チャペルヒル校で博士研究員），同安全性生物試験研究センター病理部室長，同生物薬品部室長，同生物薬品部長を経て2006年4月より現職．◇専門領域：医薬品評価科学（一般薬理，薬物代謝，化学物質リスクアセスメント，細胞毒性評価法開発，顕微鏡画像解析法開発，細胞内生化学現象の可視化技術開発，生物薬品特性解析法開発，製剤評価法開発）

Journal of Cellular Physiology

Granulocyte Colony-Stimulating Factor Promotes the Translocation of Protein Kinase Cι in Neutrophilic Differentiation Cells

TOSHIE KANAYASU-TOYODA,[1] TAKAYOSHI SUZUKI,[1] TADASHI OSHIZAWA,[1] ERIKO UCHIDA,[2] TAKAO HAYAKAWA,[2] AND TERUHIDE YAMAGUCHI[1]*

[1]*Division of Cellular and Gene Therapy Products, National Institute of Health Sciences, Tokyo, Japan*

[2]*National Institute of Health Sciences, Tokyo, Japan*

Previously, we suggested that the phosphatidylinositol 3-kinase (PI3K)-p70 S6 kinase (p70 S6K) pathway plays an important role in granulocyte colony-stimulating factor (G-CSF)-dependent enhancement of the neutrophilic differentiation and proliferation of HL-60 cells. While atypical protein kinase C (PKC) has been reported to be a regulator of p70 S6K, abundant expression of PKCι was observed in myeloid and lymphoid cells. Therefore, we analyzed the participation of PKCι in G-CSF-dependent proliferation. The maximum stimulation of PKCι was observed from 15 to 30 min after the addition of G-CSF. From 5 to 15 min into this lag time, PKCι was found to translocate from the nucleus to the membrane. At 30 min it re-translocated to the cytosol. This dynamic translocation of PKCι was also observed in G-CSF-stimulated myeloperoxidase-positive cells differentiated from cord blood cells. Small interfering RNA for PKCι inhibited G-CSF-induced proliferation and the promotion of neutrophilic differentiation of HL-60 cells. These data indicate that the G-CSF-induced dynamic translocation and activation processes of PKCι are important to neutrophilic proliferation.

J. Cell. Physiol. 211: 189–196, 2007.

Hematopoietic cell differentiation is regulated by a complex network of growth and differentiation factors (Tenen et al., 1997; Ward et al., 2000). Granulocyte colony-stimulating factor (G-CSF) and its receptors are pivotal to the differentiation of myeloid precursors into mature granulocytes. In previous studies (Kanayasu-Toyoda et al., 2002) on the neutrophilic differentiation of HL-60 cells treated with either dimethyl sulfoxide (DMSO) or retinoic acid (RA), heterogeneous transferrin receptor (Trf-R) populations—transferrin receptor-positive ($Trf\text{-}R^+$) cells and transferrin receptor-negative ($Trf\text{-}R^-$) cells—appeared 2 days after the addition of DMSO or RA. The $Trf\text{-}R^+$ cells were proliferative-type cells that had higher enzyme activity of phosphatidylinositol 3-kinase (PI3K) and protein 70 S6 kinase (p70 S6K), whereas the $Trf\text{-}R^-$ cells were differentiation-type cells of which Tyr705 in STAT3 was much more phosphorylated by G-CSF. Inhibition of either PI3K by wortmannin or p70 S6K by rapamycin was found to eliminate the difference in differentiation and proliferation abilities between $Trf\text{-}R^+$ and $Trf\text{-}R^-$ cells in the presence of G-CSF (Kanayasu-Toyoda et al., 2002). From these results, we concluded that proteins PI3K and p70 S6K play important roles in the growth of HL-60 cells and negatively regulate neutrophilic differentiation. On the other hand, the maximum kinase activity of PI3K was observed at 5 min after the addition of G-CSF (Kanayasu-Toyoda et al., 2002) and that of p70 S6K was observed between 30 and 60 min after, indicating a lag time between PI3K and p70 S6K activation. It is conceivable that any signal molecule(s) must transduce the G-CSF signal during the time lag between PI3K and p70 S6K. Chung et al. (1994) also showed a lag time between PI3K and p70 S6K activation on HepG2 cells stimulated by platelet-derived growth factor (PDGF), suggesting that some signaling molecules also may transduce between PI3K and p70S6K.

Protein kinase C (PKC) is a family of Ser/Thr kinases involved in the signal transduction pathways that are triggered by numerous extracellular and intracellular stimuli. The PKC family has been shown to play an essential role in cellular functions, including mitogenic signaling, cytoskeleton rearrangement, glucose metabolism, differentiation, and the regulation of cell survival and apoptosis. Eleven different members of the PKC family have been identified so far. Based on their structural similarities and cofactor requirements, they have been grouped into three subfamilies: (1) the classical or conventional PKCs (cPKCα, β_1, β_2, and γ), activated by Ca^{2+}, diacylglycerol, and phosphatidyl-serine; (2) the novel PKCs (nPKCδ, ε, η, and θ), which are independent of Ca^{2+} but still responsive to diacylglycerol; and (3) the atypical PKCs (aPKCζ and ι/λ), where PKCλ is the homologue of human PKCι. Atypical PKCs differ significantly from all other PKC family

Abbreviations: DMSO, dimethyl sulfoxide; fMLP-R, formyl-Met-Leu-Phe receptor; RA, retinoic acid; G-CSF, granulocyte colony-stimulating factor; Trf-R, transferrin receptor; BSA, bovine serum albumin; FITC, fluorescein isothiocyanate; PBS, phosphate-buffered saline; PKC, protein kinase C; PI3K, phosphatidylinositol 3-kinase; p70 S6K, protein 70 S6 kinase; SDS-PAGE, sodium dodecyl sulfate-polyacrylamide gel electrophoresis; siRNA, small interfering RNA; PMN, polymorphonuclear leukocyte.

Contract grant sponsor: Ministry of Health, Labor, and Welfare of Japan.

Contract grant sponsor: Ministry of Education, Culture, Sports, Science, and Technology of Japan.

*Correspondence to: Teruhide Yamaguchi, Division of Cellular and Gene Therapy Products, National Institute of Health Sciences, 1-18-1, Kamiyoga, Setagaya-ku, Tokyo 158-8501, Japan.
E-mail: yamaguch@nihs.go.jp

Received 31 May 2006; Accepted 22 September 2006

Published online in Wiley InterScience (www.interscience.wiley.com.), 28 November 2006.
DOI: 10.1002/jcp.20930

members in their regulatory domains, in that they lack both the calcium-binding domain and one of the two zinc finger motifs required for diacylglycerol binding (Liu and Heckman, 1998). Romanelli et al. (1999) reported that p70 S6K is regulated by PKCζ and participates in a PI3K-regulated signaling complex. On the other hand, Selbie et al. (1993) reported that the tissue distribution of PKCζ is different from that of PKCι/λ, and that PKCι/λ appears to be widely expressed. If the p70 S6K could be activated by aPKC, the regulation of p70 S6K activation would seem to depend on the tissue-specific expression of PKCι and/or PKCζ. In neutrophilic lineage cells, the question is which aPKC participates in the regulation of p70 S6K on G-CSF signaling.

In this study, we show that G-CSF activated PKCι, promoting its translocation from the nucleus to the cell surface membrane and subsequently to the cytosol in DMSO-treated HL-60 cells. We also show the translocation of PKCι using myeloperoxidase-positive neutrophilic lineage differentiated from cord blood, which is a rich source of immature myeloid cells (Fritsch et al., 1993; Rappold et al., 1997; Huang et al., 1999; Debili et al., 2001; Hao et al., 2001). We concluded that PKCι translocation and activation by G-CSF are needed for neutrophilic proliferation.

Materials and Methods

Reagents

Anti-p70 S6K polyclonal antibody was obtained from Santa Cruz Biotechnology (Santa Cruz, CA). Anti-PKCι polyclonal antibody and monoclonal antibody were purchased from Santa Cruz Biotechnology and from Transduction Laboratories (Lexington, KY), respectively. Anti-PKCζ polyclonal antibody was purchased from Cell Signaling Technology (Beverly, MA). Anti-myeloperoxidase antibody was purchased from Serotec Ltd. (Oxford, UK). GF 109203X, and Gö 6983 were obtained from Calbiochem-Novabiochem (San Diego, CA). Wortmannin was obtained from Sigma Chemical (St. Louis, MO). Anti-Histon-H1 antibody, anti-Fcγ receptor IIa (CD32) antibody, and anti-lactate dehydrogenase antibody were from Upstate Cell Signaling Solutions (Lake Placid, NY), Lab Vision Corp. (Fremont, CA), and Chemicon International, Inc. (Temecula, CA), respectively.

Cell culture

HL-60, Jurkut, K562, U937, and THP-1 cells were kindly supplied by the Japanese Collection of Research Bioresources Cell Bank (Osaka, Japan). Cells were maintained in RPMI 1640 medium containing 10% heat-inactivated FBS and 30 mg/L kanamycin sulfate at 37°C in moisturized air containing 5% CO_2. The HL-60 cells, which were at a density of 2.5×10^5 cells/ml, were differentiated by 1.25% DMSO. Two days after the addition of DMSO, the G-CSF-induced signal transduction was analyzed using either magnetically sorted cells or non-sorted cells.

Magnetic cell sorting

To prepare Trf-R^- and Trf-R^+ cells, magnetic cell sorting was performed as previously reported (Kanayasu-Toyoda et al., 2002), using an automatic cell sorter (AUTO MACS; Miltenyi Biotec, Bergisch Gladbach, Germany). After cell sorting, both cell types were used for Western blotting and PKCι enzyme activity analyses.

Preparation of cell lysates and immunoblotting

For analysis of PKCι and PKCζ expression, a PVDF membrane blotted with 50 μg of various tissues per lane was purchased from BioChain Institute (Hayward, CA). Both a polymorphonuclear leukocytes (PMNs) fraction and a fraction containing lymphocytes and monocytes were isolated by centrifugation (400g, 25 min) using a Mono-poly resolving medium (Dai-Nippon Pharmaceutical, Osaka, Japan) from human whole blood, which was obtained from a healthy volunteer with informed consent. T-lymphocytes were further isolated from the mixture fraction using the Pan T Cell Isolation Kit (Miltenyi Biotec) according to the manufacturer's protocol. T-lymphocytes, PMNs, HL-60 cells, Jurkut cells, K562 cells, and U937 cells (1×10^7) were collected and lysed in lysis buffer containing 1% Triton X-100, 10 mM K_2HPO_4/KH_2PO_4 (pH 7.5), 1 mM EDTA, 5 mM EGTA, 10 mM $MgCl_2$, and 50 mM β-glycerophosphate, along with 1/100 (v/v) protease inhibitor cocktail (Sigma Chemical) and 1/100 (v/v) phosphatase inhibitor cocktail (Sigma Chemical). The cellular lysate of 10^6 cells per lane was subjected to Western blotting analysis. Human cord blood was kindly supplied from the Metro Tokyo Red Cross Cord Blood Bank (Tokyo, Japan) with informed consent. Mononuclear cells, isolated with the Lymphoprep™ Tube (Axis-Shield PoC AS, Oslo, Norway), were cultured in RPMI 1640 medium containing 10% FBS in the presence of G-CSF for 3 days. Cultured cells were collected, and the cell lysate was subjected to Western blotting analysis.

A fraction of the plasma membrane, cytosol, and nucleus of the DMSO-treated HL-60 cells was prepared by differential centrifugation after the addition of G-CSF, as described previously (Yamaguchi et al., 1999). After the cells that had been suspended in 250 mM sucrose/10 mM Tris-HCl (pH 7.4) containing 1/100 (v/v) protease inhibitor cocktail (Sigma Chemical) were gently disrupted by freezing and thawing, they were centrifuged at 800g, 4°C for 10 min. The precipitation was suspended in 10 mM Tris-HCl (pH 6.7) supplemented with 1% SDS. It was then digested by benzon nuclease at 4°C for 1 h and used as a sample of the nuclear fraction. After the post-nucleus supernatant was re-centrifuged at 100,000 rpm (452,000g) at a temperature of 4°C for 40 min, the precipitate was used as a crude membrane fraction and the supernatant as a cytosol fraction. Western blotting analysis was then performed as described previously (Kanayasu-Toyoda et al., 2002). The bands that appeared on x-ray films were scanned, and the density of each band was quantitated by Scion Image (Scion, Frederick, MD) using the data from three separate experiments.

Kinase assay

The activity of PKCι was determined by phosphorous incorporation into the fluorescence-labeled pseudosubstrate (Pierce Biotechnology, Rockford, IL). The cell lysates were prepared as described above and immunoprecipitated with the anti-PKCι antibody. Kinase activity was measured according to the manufacturer's protocol. In the analysis of inhibitors effects, cells were pretreated with a PI3K inhibitor, wortmannin (100 nM), or PKC inhibitors, GF109207X (10 μM) and Gö6983 (10 μM) for 30 min, and then stimulated by G-CSF for 15 min.

Observation of confocal laser-scanning microscopy

Upon the addition of G-CSF, PKCι localization in the DMSO-treated HL-60 cells for 2 days was examined by confocal laser-activated microscopy (LSM 510, Carl Zeiss, Oberkochen, Germany). The cells were treated with 50 ng/ml G-CSF for the indicated periods and then fixed with an equal volume of 4.0% paraformaldehyde in PBS(−). After treatment with ethanol, the fixed cells were labeled with anti-PKCι antibody and with secondary antibody conjugated with horseradish peroxidase. They were then visualized with TSA™ Fluorescence Systems (PerkinElmer, Boston, MA).

Mononuclear cells prepared from cord blood cells were cultured in RPMI 1640 medium containing 10% FBS in the presence of G-CSF for 7 days. Then, for serum and G-CSF starvation, cells were cultured in RPMI 1640 medium containing 1% BSA for 11 h. After stimulation by 50 ng/ml G-CSF, the cells were fixed, stained with both anti-PKCι polyclonal antibody and anti-myeloperoxidase monoclonal antibody, and finally visualized with rhodamine-conjugated anti-rabbit IgG and FITC-conjugated anti-mouse IgG, respectively.

RNA interference

Two pairs of siRNAs were chemically synthesized: annealed (Dharmacon RNA Technologies, Lafayette, CO) and transfected into HL-60 cells using Nucleofector™ (Amaxa, Cologne, Germany). The sequences of sense siRNAs were as follows: PKCι, GAAGAAGCCUUUAGACUUUTA; p70 S6K, GCAAGGAGUCUAUCCAUGAUU. As a control, the sequence ACUCUAUCGCCAGCGUGACUU was used. Forty-eight hours after treatment with siRNA, the cells were lysed for Western blot analysis. For proliferation and differentiation assay, cells were transfected with siRNA on the first day, treated with DMSO on the second day, and supplemented with G-CSF on the third day. After cells were subsequently cultured for 5 days, cell numbers and formyl-Met-Leu-Phe receptor (fMLP-R) expression were determined.

fMLP-R expression

The differentiated cells were collected and incubated with FITC-conjugated fMLP; then, labeled cells were subjected to flow cytometric analysis (FACSCalibur, Becton Dickinson, Franklin Lakes, NJ).

Statistical analysis

Statistical analysis was performed using unpaired Student's *t*-test. Values of $P < 0.05$ were considered to indicate statistical significance. Each experiment was repeated at least three times and representative data were indicated.

Results

The distribution of atypical PKC in various tissues and cells

Previously, we reported that the PI3K-p70 S6K-cMyc pathway plays an important role in the G-CSF-induced proliferation of DMSO-treated HL-60 cells, not only by enhancing the activity of both PI3K and p70 S6K but also by inducing the c-Myc protein (Kanayasu-Toyoda et al., 2002, 2003). We also reported that G-CSF did not stimulate Erk1, Erk2, or 4E-binding protein 1. The maximum kinase activity of PI3K was observed 5 min after the addition of G-CSF, and that of p70 S6K was observed between 30 and 60 min after. It is conceivable that any signal molecule(s) must transduce the G-CSF signal during the time lag between PI3K and p70 S6K. Romanelli et al. (1999) suggested that the activation of p70 S6K is regulated by PKCξ and participates in the PI3K-regulated signaling complex. To examine the role of atypical PKC in the G-CSF-dependent activation and the relationship between atypical PKC and p70 S6K, the protein expression of PKCζ and PKCι in various human tissues and cells was analyzed by Western blotting. As shown in Figure 1A, both of the atypical PKCs were markedly expressed in lung and kidney but were weakly expressed in spleen, stomach, and placenta. In brain, cervix, and uterus, the expression of only PKCι was observed. Selbie et al. (1993) have reported observing the expression of PKCζ not in protein levels but in RNA levels, in the kidney, brain, lung, and testis, and that of PKCι in the kidney, brain, and lung. In this study, the protein expression of PKCι in the kidney, brain, and lung was consistent with the RNA expression of PKCι. Despite the strong expression of PKCζ RNA in brain (Selbie et al., 1993), PKCζ protein was scarcely observed. Although PKCι proteins were scarcely expressed in neutrophils and T-lymphocytes in peripheral blood, they were abundantly expressed in immature blood cell lines, that is, Jurkut, K562, U937, and HL-60 cells (Fig. 1B), in contrast with the very low expression of PKCζ proteins. In mononuclear cells isolated from umbilical cord blood, which contains large numbers of immature myeloid cells and has a high proliferation ability, the expression of PKCι proteins was also observed. Since Nguyen and Dessauer (2005) have reported observing abundant PKCζ proteins in THP-1 cells, as a positive control for PKCζ, we also performed a Western blot of THP-1 cells (Fig. 1B, right part). While PKCι was markedly expressed in both THP-1 and HL-60 cells, PKCζ was observed only in THP-1 cells.

These data suggested that PKCζ and PKCι were distributed differently in various tissues and cells, and that mainly PKCι proteins were expressed in proliferating blood cells.

Stimulation of PKCι activity by G-CSF

Among the 11 different members of the PKC family, the aPKCs (ζ and ι/λ) have been reported to activate p70 S6K activity and to be regulated by PI3K (Akimoto et al., 1998; Romanelli et al., 1999). As shown in Figure 1, although the PKCζ proteins were not detected by Western blotting in HL-60 cells or mononuclear cells isolated from cord blood cells, it is possible that PKCι could functionally regulate p70 S6K as an upstream regulator in these cells. Therefore, we focused on the role of PKCι as the possible upstream regulator of p70 S6K in neutrophil lineage cells. First, we compared the expression of PKCι in both Trf-R^+ and Trf-R^- cells. PKCι proteins were expressed more abundantly in Trf-R^+ cells than in Trf-R^- cells (Fig. 2A, middle part), as with the p70 S6K proteins. A time course study of PKCι activity upon the addition of G-CSF revealed the maximum stimulation at 15 min, lasting until 30 min. The G-CSF-dependent activation of PKCι was inhibited by the PKC inhibitors wortmannin, GF 109203X, and Gö 6983. Considering the marked inhibitory effect of wortmannin on PKCι and evidence that the maximum stimulation of PI3K was observed at 5 min after the addition of G-CSF, PI3K was determined to be the upstream regulator of PKCι in the G-CSF signal transduction of HL-60 cells. The basal activity of PKCι in Trf-R^+ cells was higher than that in Trf-R^- cells, and G-CSF was more augmented. In Trf-R^- cells, PKCι activity was scarcely stimulated by G-CSF. This tendency of PKCι to be activated by G-CSF was similar to that of PI3K (Kanayasu-Toyoda et al., 2002).

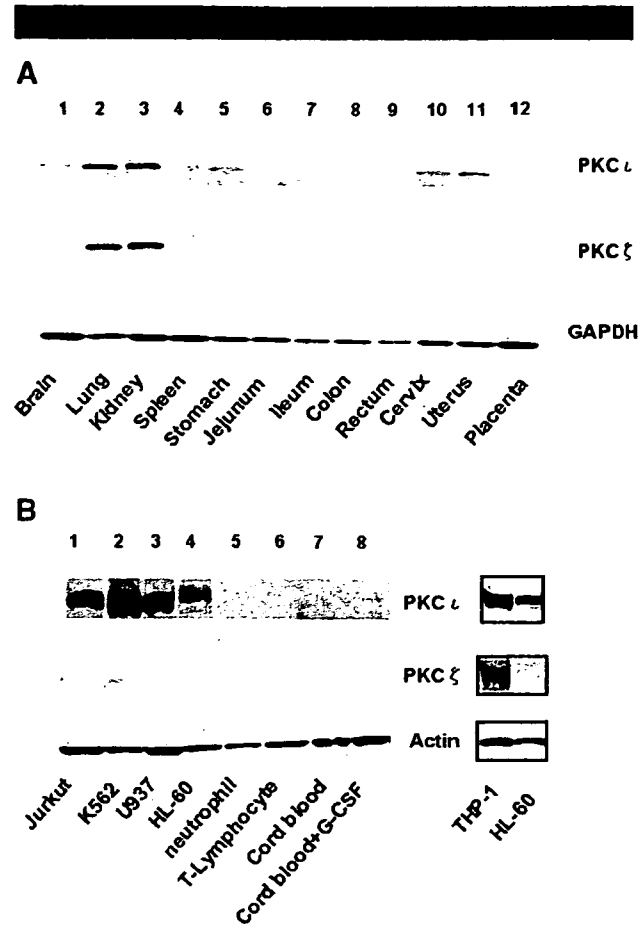

Fig. 1. Different distributions of PKCζ and PKCι. The protein expression of PKCι appears in the upper part and that of PKCζ in the middle part in various tissues and cells. A: 1, brain; 2, lung; 3, kidney, 4, spleen; 5, stomach; 6, jejunum; 7, ileum; 8, colon; 9, rectum; 10, cervix; 11, uterus; 12, placenta. Anti-GAPDH blot is a control for various tissues. B: 1, jurkut cells; 2, K562 cells; 3, U937 cells; 4, HL-60 cells; 5, neutrophils; 6, T-lymphocytes; 7, mononuclear cells from cord blood in the absence of G-CSF; 8, mononuclear cells from cord blood in the presence of G-CSF. Anti-actin blot is a control. The right part shows immunoblots of PKCι, PKCζ, and actin of THP-1 cells as a positive control for PKCζ. The cell numbers of THP-1 and HL-60 cells were adjusted in relation to other cells on the left parts.